

Energy and waiting time distributions of FRB 121102 observed by FASTG. Q. ZHANG,¹ P. WANG,² Q. WU,¹ F. Y. WANG,^{1,3} D. LI,² Z. G. DAI,^{4,1} AND B. ZHANG⁵¹*School of Astronomy and Space Science, Nanjing University, Nanjing 210093, China*²*CAS Key Laboratory of FAST, NAOC, Chinese Academy of Sciences, Beijing 100101, China*³*Key Laboratory of Modern Astronomy and Astrophysics (Nanjing University), Ministry of Education, Nanjing 210093, China*⁴*Department of Astronomy, School of Physical Sciences, University of Science and Technology of China, Hefei 230026, China*⁵*Department of Physics and Astronomy, University of Nevada, Las Vegas, Las Vegas, NV 89154, USA*

Submitted to ApJL

ABSTRACT

The energy and waiting time distributions are important properties to understand the physical mechanism of repeating fast radio bursts (FRBs). Recently, Five-hundred-meter Aperture Spherical radio Telescope (FAST) detected the largest sample of FRB 121102, containing 1652 bursts. The energy distribution at high-energy range ($> 10^{38}$ erg) can be fitted with a single power-law function with an index of -1.86 . However, the distribution at low-energy range deviates from the power-law function. The energy distributions of high-energy bursts at different epochs are inconsistent. We find the power-law index of -1.70 for early bursts and -2.60 for later bursts. For bursts observed in a single day, a linear repetition pattern is found. We use the Weibull function to fit the waiting time distribution. The shape parameter $k = 0.72_{-0.02}^{+0.01}$ and the event rate $r = 734.47_{-27.58}^{+29.04}$ day⁻¹ are derived. If the waiting times with $\delta_t < 28$ s are excluded, the burst behavior can be described by a Poisson process. The best-fitting values of k are slightly different for low-energy and high-energy bursts. The event rates change significantly across the observing time, while the shape parameters k vary slightly in different days.

Keywords: Radio bursts; Radio transient sources

1. INTRODUCTION

Fast radio bursts (FRBs) are bright bursts at radio frequency with milliseconds-duration (for reviews, see Cordes & Chatterjee 2019; Petroff et al. 2019; Zhang 2020; Xiao et al. 2021). According to their burst behavior, FRBs can be divided into two classes: repeating FRBs and apparently non-repeating FRBs. There are more than twenty repeating FRBs detected so far, with FRB 121102

(Spitler et al. 2016) and FRB 180916 (CHIME/FRB Collaboration et al. 2019) being examples. Whether all FRBs are repeating sources is still under debate (Palaniswamy et al. 2018; Caleb et al. 2019; Ravi 2019; Ai et al. 2021). The repeating behavior excludes some catastrophe models. Recently, FRB 200428 was found to be associated with a Galactic magnetar SGR 1935+2154 (CHIME/FRB Collaboration et al. 2020a; Bochenek et al. 2020), which supports that at least a part of FRBs are produced by magnetars. Some models have been proposed to interpret how magnetars may produce FRBs (Popov & Postnov 2013; Kulkarni et al. 2014; Murase et al. 2016; Katz 2016; Beloborodov 2017; Lu & Kumar 2018; Yang & Zhang 2018; Metzger et al. 2019; Wadiasingh & Timokhin 2019; Wang et al. 2020; Lu et al. 2020; Yang & Zhang 2021).

FRB 121102 is the first detected repeating FRB, which has been observed from 400 MHz to 8 GHz (Spitler et al. 2014, 2016; Chatterjee et al. 2017; Michilli et al. 2018; Gajjar et al. 2018). In the past few years, about 300 bursts have been observed from this source. The high burst rate enables it being investigated extensively. It was localized in a star-forming region in a dwarf galaxy in association with a persistent radio source (Chatterjee et al. 2017; Marcote et al. 2017; Tendulkar et al. 2017a). The repeating bursts from FRB 121102 as an extreme value of the rotation measure RM (Michilli et al. 2018).

The energy distribution of repeating FRBs provides a clue to understand the physical mechanism to produce FRBs. Wang & Yu (2017) first found that the differential energy distribution of FRB 121102 is $dN/dE \propto E^{-1.8 \pm 0.15}$. Law et al. (2017a) estimated that the energy distribution of FRB 121102 satisfies a simple power-law distribution with $dN/dE \propto E^{-1.7}$. However, Gourdji et al. (2019) derived a power-law index of about -2.7 . They argued that the difference between these results are caused by the incompleteness at low energies. Wang & Zhang (2019) used the cut-off power-law function to fit bursts observed by multiple observations and found that the power-law indices of different observations are close to -1.7 . The Apertif data suggested a slope of -2.7 above the completeness threshold $\sim 10^{39}$ erg (Oostrum et al. 2020). An index -2.1 ± 0.1 was found by Cruces et al. (2021) using the bursts detected by Effelsberg telescope. Therefore, the energy distribution of FRB 121102 has been controversial. To have a better understanding of the energy distribution, more bursts spanning a large energy range are required.

Although many bursts of FRB 121102 have been observed, the burst behavior is still confusing. A possible long-term period has been discovered for FRB 121102. Rajwade et al. (2020) derived a period about 156.9 days. This result was examined by Cruces et al. (2021). They found a period of about 161 days, which is consistent with the result of Rajwade et al. (2020). The similar periodic behavior (with a period of ~ 16 days) was discovered earlier for FRB 180916 (CHIME/FRB Collaboration et al. 2020b). Many models have been proposed to explain this periodic behavior, including binary star models (Ioka & Zhang 2020; Dai & Zhong 2020; Lyutikov et al. 2020; Deng et al. 2021; Kuerban et al. 2021; Wada et al. 2021), precession models (Zanazzi & Lai 2020; Levin et al. 2020; Yang & Zou 2020), and ultra-long period magnetar models (Beniamini et al. 2020).

No shorter period has been discovered for FRB 121102 (Zhang et al. 2018; Li et al. 2021). Wang & Yu (2017) first found that the repetition pattern of FRB 121102 cannot be described by a Poisson process. A similar conclusion was drawn by Oppermann et al. (2018). They also suggested that a Weibull function is suitable to describe the distribution of the waiting times. The shape parameter k is derived as $k = 0.34$, which means that the bursts of FRB 121102 tend to cluster in time. Oostrum et al. (2020) also used the Weibull function to fit the burst behavior and obtained $k = 0.49$. A

higher shape parameter $k = 0.82$ was derived by Cruces et al. (2021). It is obvious that the value of k varies significantly from different observations. Meanwhile, the burst rate depends on telescope sensitivity. The burst rate of low-energy bursts is crucial to understand the repetition behavior of repeating FRBs.

Recently, the Five-hundred-meter Aperture Spherical Telescope (FAST) detected 1652 bursts from FRB 121102 (Li et al. 2021), which is the largest burst sample for this source. The high sensitivity of FAST enables it to detect many low-energy bursts, which are difficult to detect with other telescopes. This large sample is helpful to reveal the properties of FRB 121102. Li et al. (2021) reported the bimodal energy distribution. More interestingly, there are three obvious peaks in the kernel density estimation (KDE) of energy and burst time (as shown in the panel (c) of their Figure 1). The high energy peak is only visible in early observations, while the low energy peaks exist in both early and late observations (Li et al. 2021).

In this paper, we use FAST burst sample to investigate the energy distribution and burst behavior of FRB 121102. This paper is organized as follows. In Section 2, we introduce the data and derive the energy distribution. The Weibull function is used to fit the waiting time distribution. The discussion is presented in Section 3 and conclusions are drawn in Section 4.

2. DATA AND RESULTS

2.1. Data

FRB 121102 has been observed by different telescopes (Spitler et al. 2014, 2016; Scholz et al. 2016, 2017; Chatterjee et al. 2017; Law et al. 2017a; Hardy et al. 2017; Zhang et al. 2018; Spitler et al. 2018; Gajjar et al. 2018; Michilli et al. 2018; Gourdji et al. 2019; Hessels et al. 2019; Oostrum et al. 2020; Caleb et al. 2020; Cruces et al. 2021). Recently, FAST observed this source at 1.25 GHz (Li et al. 2021). The observations were carried out from August 2019 to October 2019, a duration almost covering the entire active phase of a period. During the 59.5 observing hours, FAST detected 1652 bursts. The mean burst rate was about 27.8 hr^{-1} , and the peak burst rate was 122 hr^{-1} . These bursts help to understand the energy distribution in both low-energy and high-energy ranges. The waiting time distribution can be studied in detail with this sample. We will use this sample to derive a more precise waiting time distribution and investigate the dependence of waiting time on observing time.

2.2. Energy Distribution

The energy distribution of FRB 121102 has been investigated by many previous works (Wang & Yu 2017; Law et al. 2017a; Gourdji et al. 2019; Wang & Zhang 2019; Cheng et al. 2020a; Oostrum et al. 2020; Cruces et al. 2021; Li et al. 2021). We use the bursts of FRB 121102 observed by FAST to investigate the differential energy distribution

$$dN/dE \propto E^{-\alpha_E}. \quad (1)$$

The energies of these bursts are listed in Li et al. (2021). Central frequency rather than bandwidth is used to calculate the energy of a burst (e.g. Zhang 2018). The luminosity distance of FRB 121102 is taken as 949 Mpc (Planck Collaboration & et al. 2016; Tendulkar et al. 2017b). We show the probability energy distribution as blue histogram in Figure 1. The low-energy distribution deviates from the simple power-law distribution. Therefore, in order to compare with previous works, we

only consider the high-energy bursts ($E > 10^{38}$ erg). There are about 600 bursts in the high-energy range ($E > 10^{38}$ erg). The distribution can be approximated as a simple power-law function. We use equation (1) to fit the energy distribution in the high-energy end. The fitting result is shown as the green dot-dashed line in Figure 1. The power-law index is $\alpha_E = 1.86 \pm 0.02$, which is very consistent with the index derived by Wang & Yu (2017). Law et al. (2017a) obtained a power-law index of $\alpha_E \simeq 1.7$, which is also consistent with our result. Wang & Zhang (2019) used a cut-off power-law model to fit the FRB 121102 data from multiple observations and derived a universal energy distribution with $\alpha_E = 1.6 - 1.8$ for different observations at different frequencies. Our result also falls in this range. The energy distribution of high-energy bursts was also investigated by Li et al. (2021). Because the observation of FAST for FRB 121102 consists of many single-day observations, Li et al. (2021) used various observational times as the weight to derive the differential burst rate dR/dE at different energies and found a power-law index of about -1.85 ± 0.3 . Our result is the distribution of burst counts in each energy bin dN/dE , not the burst rate distribution dR/dE .

Interestingly, the energies of non-repeating FRBs also show a power-law distribution with $\alpha_E = 1.6 - 1.8$ (Cao et al. 2018; Lu & Piro 2019; Zhang et al. 2019, 2021). Some sources also show a power-law distribution of dN/dE , such as X-ray bursts of magnetars (Gögüş et al. 2000; Prieskorn & Kaaret 2012; Cheng et al. 2020b; Yang et al. 2021), X-ray flares of gamma-ray bursts (Wang & Dai 2013), M87 (Yang et al. 2019) and Sgr A* (Wang et al. 2015; Li et al. 2015). Some FRB theoretical models are related to giant pulses of pulsars (e.g. Cordes & Wasserman 2016). The giant pulses of Crab pulsar also show a power-law distribution (Popov & Stappers 2007; Lyu et al. 2021). A power-law distribution of energy is a natural predication of self-organized criticality theory (Bak et al. 1987; Aschwanden 2011).

The energy distribution in low-energy range deviates from this power-law. This deviation was also reported by Gourdji et al. (2019). They attributed this deviation to the incompleteness at low energies. In our sample, the turning point is about 10^{38} erg, much larger than the threshold energy, which is about 3×10^{37} erg (Li et al. 2021). Therefore, this deviation is physical. It indicates that more than one physical mechanisms or emission sites are likely operating to generate bursts. The distribution also shows an obvious steepening above $E > 5 \times 10^{39}$ erg, which indicates the burst maximum energy E_{\max} is around this point. A similar deviation was also found in other samples (Wang & Zhang 2019; Oostrum et al. 2020; Cruces et al. 2021). Li et al. (2021) also investigated the energy distribution of FRB 121102. They found the bimodal energy distribution. They also give the KDE of energy and burst time in the panel (c) of their Figure 1. In this panel, the high-energy component is only visible in early observations, while the low-energy peaks are present in both early and later observations. This novel structure may suggest different physical mechanisms for high-energy and low-energy bursts. If this conjecture is true, it can explain the deviation in low energies.

2.3. Waiting time Distribution

The burst behavior of FRB 121102 does not follow the Poisson distribution (Wang & Yu 2017). Oppermann et al. (2018) used the Weibull function to describe the burst behavior of FRB 121102, which is

$$\mathcal{W}(\delta_t | k, r) = k\delta_t^{-1}[\delta_t r \Gamma(1 + 1/k)]^k e^{-[\delta_t r \Gamma(1 + 1/k)]^k}, \quad (2)$$

where δ_t is the waiting time, k is the shape parameter, r is the mean burst rate, and Γ is the gamma function. The case for $k = 1$ corresponds to the Poisson distribution. Previous works suggested that the repeating behavior of FRB 121102 tends to have $k < 1$ (Oppermann et al. 2018; Oostrum et al. 2020; Cruces et al. 2021), which means that time clustering is favored. We use the Weibull function to fit the burst behavior of the FAST sample. The observations of FAST lasted for about 1 hour each day. Therefore, waiting times greater than half day is caused by the observing window, which is ignored in our analysis. The waiting time with $\delta_t < 30$ ms is also excluded. It is difficult to determine whether they are two separate bursts or multiple peaks of a single burst. We use the MCMC (Markov chain Monte Carlo) technique to fit this distribution. The corner plot of the best-fitting results is shown in Figure 2. We list the best-fitting parameters in Table 1. The results of the previous works are also listed in this table. We find $k = 0.72_{-0.02}^{+0.01}$ and $r = 734.47_{-27.58}^{+29.04} \text{ day}^{-1}$. This burst rate is much higher than the rates derived in previous works, which is caused by the high sensitivity of FAST. The cumulative distribution of waiting time is shown in Figure 3. The green dashed line is the predicted result of the Weibull function and the dot-dashed red line is predicted by the Poisson process. The Weibull function is better than the Poisson function in fitting the results.

Oppermann et al. (2018) collected 17 bursts observed by Arecibo, Effelsberg, GBT, VLA, and Lovell. They derived $k = 0.34$ with these 17 bursts. Oostrum et al. (2020) obtained $k = 0.49$. Their results are smaller than ours. This may be caused by the low waiting time cutoff. Cruces et al. (2021) found that when exclude the waiting time $\delta_t < 1$ s, the shape parameter k shifts from $k = 0.62$ to $k = 0.73$. We carefully check the effect of waiting time cutoff $\delta_{t,c}$ and show the dependence of k on $\delta_{t,c}$ in Figure 4. The solid blue line is the evolution of k and the vertical solid blue lines are 1σ errors. The shape parameter k increases as $\delta_{t,c}$ increases. When $\delta_{t,c} \simeq 28$ s, the shape parameter k is close to 1, which means that the repeating behavior is due to the Poisson process. Cruces et al. (2021) also found that the waiting time with $\delta_t > 100$ s is consistent with the Poisson process, which is similar to our results.

2.4. Linear repetition pattern

We use the FAST data to check the burst repetition pattern. We select the single-day observations with the number of detected bursts larger than 60 and show the cumulative distribution function with blue scatters in each panel of Figure 5. The observation time is listed in each panel. We find that the distribution can be fitted with a linear function

$$N(< t) = kt + b. \quad (3)$$

The best-fitting results with the dashed red lines are in each panel and the best-fitting parameters are also listed. The observations on 2019-09-07 is a little different. There is a clear gap between early bursts and later ones. The later bursts can be fitted well with Equation (3). Although the fitting results are different, they can be all fitted with equation 3. Tabor & Loeb (2020) proposed that the burst rate is constant per logarithmic time. The observations of GBT was used in their analysis (Zhang et al. 2018). They found that the cumulative distribution function can be fitted with $N(< t) = \alpha \ln(t/t_0)$ rather than $N \propto t$. Our result is different from theirs. A linear repetition pattern, strongly favored by FAST observation, would give strict constraints on theoretical models.

3. DISCUSSION

3.1. Energy distribution in different epochs

An important conclusion of Li et al. (2021) is the novel triple peaks structure in the KDE of energy and burst time (As shown in the panel (c) of their Figure 1). There is a clear gap between the high-energy bursts and low-energy bursts in the early phase. The gap between early bursts and late bursts is also significant. Following the division of Li et al. (2021), we regard the bursts occurring before MJD 58740 as early bursts and the bursts occurring after MJD 58740 as late bursts. The energy distributions are shown in Figure 6. Again, we only fit the bursts with energy $> 10^{38}$ erg. The best-fitting results are shown as green dot-dashed lines. The power-law index for the early bursts is $-1.70_{-0.03}^{+0.03}$, while that for the late bursts is $-2.60_{-0.14}^{+0.15}$, which is very different.

Some previous works support the power-law index -1.7 (Wang & Yu 2017; Law et al. 2017b; Wang & Zhang 2019), which is consistent with the result of early bursts. However, there are also some works that suggested a steeper index (Gourdji et al. 2019), which is close to the result of late bursts. This difference may be caused by the following reason. First, the gap between early bursts and late bursts is significant. There may be different modes of burst emission operating in different epochs, so that the observed energy distribution may depend on the observing time. The two different modes may be related to different mechanisms or different emission sites. Li et al. (2021) reported the triple peaks in the distribution of energy and bursts time (as shown in panel (c) of their Figure 1). At the early epoch, the bursts with $E > 10^{38}$ erg are belong to high-energy burst component. However, the high-energy peak is invisible in the late epoch. The bursts with $E > 10^{38}$ erg in the late epoch is an extension of low-energy bursts. If the high-energy bursts and low-energy bursts originate from different mechanisms or different sites, which operate in different epochs, the variance of the energy distribution is naturally interpreted.

3.2. Waiting time for different energies

Li et al. (2021) reported the triple peaks structure in the panel (c) of their Figure 1. The bimodal structure in the energy distribution in the early phase may suggest that they are produced by different physical processes. Therefore, we wonder whether there are differences in their other properties. If the low-energy bursts and high-energy bursts are produced by different processes, the waiting time should be calculated independently. We divide all the bursts into three sub-samples: the low-energy bursts and high-energy bursts between MJD 58717 and 58740, and the late-phase bursts detected between MJD 58740 and 58776. The dividing line in burst time is consistent with the choice of Li et al. (2021). We take the dividing line between low-energy bursts and high-energy bursts as 1.58×10^{38} erg. For each sub-sample, we calculate the waiting time independently and show the count distribution in Figure 7. The peaks of low-energy bursts and the late-phase bursts are consistent with each other, which is about 60 s. The consistency of energy and waiting time between these two samples suggests that they likely have a similar physical origin. The peak of high-energy burst waiting time is little higher, which is close to 260 s. However, the difference is not significant enough.

We also use the Weibull function to fit these three sub-samples. Again, we ignore the waiting times with $\delta_t < 30$ ms and $\delta_t > 0.5$ day. We list the best-fitting results for three sub-samples in Table 1. The shape parameters are $k \simeq 0.69$ for low-energy bursts, $k \simeq 0.76$ for high-energy bursts and $k \simeq 0.66$ for late-phase bursts. The posterior distributions of k for the three sub-samples are shown in Figure 8. The k parameters for low-energy bursts, high-energy bursts, and late-phase bursts are shown as black line, red line, and blue line, respectively. The vertical dashed lines are the best-

fitting results. The shape parameters k for low-energy and later-phase bursts are consistent with each other within 1σ error, while the k parameter for high-energy bursts is higher. The consistency of low-energy bursts and late-phase bursts may suggest that they have the same origin, while the high-energy bursts may have a different origin. The difference between later-phase bursts and high-energy bursts is significant, but the variance between low-energy bursts and high-energy bursts is insignificant. This may be caused by the rough division of low-energy bursts and high-energy bursts. We simply use 1.58×10^{38} erg as the criterion. However, the count distributions of low-energy and high-energy bursts are close to a log-normal distribution. They can be extended to include each other. Therefore, some FRBs may be misclassified. If we can make a robust classification, the difference in waiting time may be larger.

We derive the burst rates for low-energy bursts and high-energy bursts are 445.35 per day and 354.74 per day, respectively. The burst rate of low-energy bursts is higher than that of high energy bursts. These two classes of bursts occurred in the same epoch. For the bursts occurring in late observation days, the burst rate is about 800.54 per day, which is higher than that of low-energy bursts and high-energy bursts, but close to the sum of these two classes of bursts.

We also check the dependence of energy on waiting time. For X-ray flares of gamma-ray bursts, an anti-correlation is found between energy and waiting time (Yi et al. 2016). The scatter plot of energy and waiting time of the FAST FRB sample is shown in Figure 9. No significant dependence of energy on waiting time is found. We also check the dependence for three sub-samples and found no significant dependence.

3.3. *Waiting time in different observational days*

The FAST observations spanned two months in time, which covered most of the active window of FRB 121102. We can test the dependence of the burst behaviors on observational time. The observations lasted for about 1 hour each day. We regard the observations in each day as single samples and select some samples with the number of the observed bursts greater than 5. Then, the Weibull function is applied to fit the waiting time distribution in these days. The best-fitting results against burst time are shown in Figure 10. The blue points are the shape parameters k with 1σ errors, and the yellow points are the burst rates r with 1σ errors. The event rate r changes significantly across observing time, while the shape parameter k varies a little in different days. It is also interesting that the value of k is close to 1 in some days, which indicates a rough Poisson distribution of the waiting time.

4. CONCLUSIONS

The energy and waiting time distributions of FRB 121102 provide a clue to understand the physical origin of repeating FRBs. FAST has detected many faint bursts from this source, which comprises the largest sample observed by a single telescope from a single source (Li et al. 2021). The detection of these faint bursts enables us to perform extensive statistical studies of the burst properties. Our conclusions can be summarized as follows.

1. The energy distribution in the high-energy range can be fitted with a simple power-law function. The power-law index is -1.86 ± 0.02 , which is consistent with previous results (Wang & Yu 2017; Law et al. 2017a; Wang & Zhang 2019; Cruces et al. 2021). However, the energy distribution deviates from this power-law function at low energies. The turning point is about 10^{38} erg,

which is larger than the instrument sensitivity threshold. Thus, this deviation is not caused by the incompleteness in the low-energy end. A different physical mechanism or different emission site for low-energy events may be required to explain this deviation.

2. The Weibull function is used to fit the waiting times excluding $\delta_t < 30$ ms and $\delta_t > 0.5$ day. We derive $k = 0.72_{-0.02}^{+0.01}$ and $r = 734.47_{-27.58}^{+29.04}$ day⁻¹. This result ($k < 1$) suggests that the bursts of FRB 121102 tend to cluster in time. We also found that when we exclude the waiting time $\delta_t < 28$ s, the burst behavior can be roughly described by a Poisson process.
3. For bursts observed in a single day, a linear repetition pattern is found. We select the observations with the observed bursts larger than 60 in one day. The cumulative distributions of the burst time are shown in Figure 5. These distributions can be fitted with $N(< t) = kt + b$.
4. The distributions of high-energy early bursts and late bursts are different. When the bursts with $E > 10^{38}$ erg are considered, the power-law index is -1.70 for early bursts and -2.60 for late bursts. This difference may suggest that they have different physical origins, with the latter the extension of the low-energy component.
5. According to the bimodal structure of energy distribution, we divide the bursts into 3 classes: the low-energy bursts and high-energy bursts between MJD 58717 and 58740, and the late-phase bursts. The waiting time distributions of the low-energy bursts and the late-phase bursts are consistent with each other. However, the peak of the waiting time distribution of high-energy bursts is somewhat higher. The posterior probability distribution of the k parameter for high-energy bursts is also slightly different from that of the low-energy and the late-phase bursts. These differences may suggest that they have different physical origins or emission sites.
6. There is no significant dependence of energy on waiting time. The scatter plot of energy and waiting time is shown in Figure 9. For three sub-samples, we also do not find any dependence between the two parameters.

ACKNOWLEDGEMENTS

This work was supported by the National Natural Science Foundation of China (grant No. 11988101, No. U1831207, No. 11833003, No. 11725313, No. 11690024, No. 12041303 and No. U2031117), the Fundamental Research Funds for the Central Universities (No. 0201-14380045), the National Key Research and Development Program of China (grant 2017YFA0402600); and the National SKA Program of China No. 2020SKA0120200, the Cultivation Project for FAST Scientific Payoff and Research Achievement of CAMS-CAS. PW acknowledges support by the Youth Innovation Promotion Association CAS (id. 2021055) and CAS Project for Young Scientists in Basic Research (grant YSBR-006). This work made use of data from FAST, a Chinese national mega-science facility built and operated by the National Astronomical Observatories, Chinese Academy of Sciences.

REFERENCES

- Ai, S., Gao, H., & Zhang, B. 2021, ApJL, 906, L5, doi: [10.3847/2041-8213/abcec9](https://doi.org/10.3847/2041-8213/abcec9)
- Aschwanden, M. J. 2011, Self-Organized Criticality in Astrophysics

- Bak, P., Tang, C., & Wiesenfeld, K. 1987, *PhRvL*, 59, 381, doi: [10.1103/PhysRevLett.59.381](https://doi.org/10.1103/PhysRevLett.59.381)
- Beloborodov, A. M. 2017, *ApJL*, 843, L26, doi: [10.3847/2041-8213/aa78f3](https://doi.org/10.3847/2041-8213/aa78f3)
- Beniamini, P., Wadiasingh, Z., & Metzger, B. D. 2020, *MNRAS*, 496, 3390, doi: [10.1093/mnras/staa1783](https://doi.org/10.1093/mnras/staa1783)
- Bochenek, C. D., Ravi, V., Belov, K. V., et al. 2020, *Nature*, 587, 59, doi: [10.1038/s41586-020-2872-x](https://doi.org/10.1038/s41586-020-2872-x)
- Caleb, M., Stappers, B. W., Rajwade, K., & Flynn, C. 2019, *MNRAS*, 484, 5500, doi: [10.1093/mnras/stz386](https://doi.org/10.1093/mnras/stz386)
- Caleb, M., Stappers, B. W., Abbott, T. D., et al. 2020, *MNRAS*, 496, 4565, doi: [10.1093/mnras/staa1791](https://doi.org/10.1093/mnras/staa1791)
- Cao, X.-F., Yu, Y.-W., & Zhou, X. 2018, *ApJ*, 858, 89, doi: [10.3847/1538-4357/aabadd](https://doi.org/10.3847/1538-4357/aabadd)
- Chatterjee, S., Law, C. J., Wharton, R. S., et al. 2017, *Nature*, 541, 58, doi: [10.1038/nature20797](https://doi.org/10.1038/nature20797)
- Cheng, Y., Zhang, G. Q., & Wang, F. Y. 2020a, *MNRAS*, 491, 1498, doi: [10.1093/mnras/stz3085](https://doi.org/10.1093/mnras/stz3085)
- . 2020b, *MNRAS*, 491, 1498, doi: [10.1093/mnras/stz3085](https://doi.org/10.1093/mnras/stz3085)
- CHIME/FRB Collaboration, Andersen, B. C., Bandura, K., et al. 2019, *ApJL*, 885, L24, doi: [10.3847/2041-8213/ab4a80](https://doi.org/10.3847/2041-8213/ab4a80)
- CHIME/FRB Collaboration, Andersen, B. C., Bandura, K. M., et al. 2020a, *Nature*, 587, 54, doi: [10.1038/s41586-020-2863-y](https://doi.org/10.1038/s41586-020-2863-y)
- CHIME/FRB Collaboration, Amiri, M., Andersen, B. C., et al. 2020b, *Nature*, 582, 351, doi: [10.1038/s41586-020-2398-2](https://doi.org/10.1038/s41586-020-2398-2)
- Cordes, J. M., & Chatterjee, S. 2019, *ARA&A*, 57, 417, doi: [10.1146/annurev-astro-091918-104501](https://doi.org/10.1146/annurev-astro-091918-104501)
- Cordes, J. M., & Wasserman, I. 2016, *MNRAS*, 457, 232, doi: [10.1093/mnras/stv2948](https://doi.org/10.1093/mnras/stv2948)
- Cruces, M., Spitler, L. G., Scholz, P., et al. 2021, *MNRAS*, 500, 448, doi: [10.1093/mnras/staa3223](https://doi.org/10.1093/mnras/staa3223)
- Dai, Z. G., & Zhong, S. Q. 2020, *ApJL*, 895, L1, doi: [10.3847/2041-8213/ab8f2d](https://doi.org/10.3847/2041-8213/ab8f2d)
- Deng, C.-M., Zhong, S.-Q., & Dai, Z.-G. 2021, arXiv e-prints, arXiv:2102.06796, <https://arxiv.org/abs/2102.06796>
- Gajjar, V., Siemion, A. P. V., Price, D. C., et al. 2018, *ApJ*, 863, 2, doi: [10.3847/1538-4357/aad005](https://doi.org/10.3847/1538-4357/aad005)
- Gourdji, K., Michilli, D., Spitler, L. G., et al. 2019, *ApJL*, 877, L19, doi: [10.3847/2041-8213/ab1f8a](https://doi.org/10.3847/2041-8213/ab1f8a)
- Gögüs, E., Woods, P. M., Kouveliotou, C., et al. 2000, *ApJL*, 532, L121, doi: [10.1086/312583](https://doi.org/10.1086/312583)
- Hardy, L. K., Dhillon, V. S., Spitler, L. G., et al. 2017, *MNRAS*, 472, 2800, doi: [10.1093/mnras/stx2153](https://doi.org/10.1093/mnras/stx2153)
- Hessels, J. W. T., Spitler, L. G., Seymour, A. D., et al. 2019, *ApJL*, 876, L23, doi: [10.3847/2041-8213/ab13ae](https://doi.org/10.3847/2041-8213/ab13ae)
- Ioka, K., & Zhang, B. 2020, *ApJL*, 893, L26, doi: [10.3847/2041-8213/ab83fb](https://doi.org/10.3847/2041-8213/ab83fb)
- Katz, J. I. 2016, *ApJ*, 826, 226, doi: [10.3847/0004-637X/826/2/226](https://doi.org/10.3847/0004-637X/826/2/226)
- Kuerban, A., Huang, Y.-F., Geng, J.-J., et al. 2021, arXiv e-prints, arXiv:2102.04264, <https://arxiv.org/abs/2102.04264>
- Kulkarni, S. R., Ofek, E. O., Neill, J. D., Zheng, Z., & Juric, M. 2014, *ApJ*, 797, 70, doi: [10.1088/0004-637X/797/1/70](https://doi.org/10.1088/0004-637X/797/1/70)
- Law, C. J., Abruzzo, M. W., Bassa, C. G., et al. 2017a, *ApJ*, 850, 76, doi: [10.3847/1538-4357/aa9700](https://doi.org/10.3847/1538-4357/aa9700)
- . 2017b, *ApJ*, 850, 76, doi: [10.3847/1538-4357/aa9700](https://doi.org/10.3847/1538-4357/aa9700)
- Levin, Y., Beloborodov, A. M., & Bransgrove, A. 2020, *ApJL*, 895, L30, doi: [10.3847/2041-8213/ab8c4c](https://doi.org/10.3847/2041-8213/ab8c4c)
- Li, D., Wang, P., Zhu, W. W., et al. 2021, arXiv e-prints, arXiv:2107.08205, <https://arxiv.org/abs/2107.08205>
- Li, Y.-P., Yuan, F., Yuan, Q., et al. 2015, *ApJ*, 810, 19, doi: [10.1088/0004-637X/810/1/19](https://doi.org/10.1088/0004-637X/810/1/19)
- Lu, W., & Kumar, P. 2018, *MNRAS*, 477, 2470, doi: [10.1093/mnras/sty716](https://doi.org/10.1093/mnras/sty716)
- Lu, W., Kumar, P., & Zhang, B. 2020, *MNRAS*, 498, 1397, doi: [10.1093/mnras/staa2450](https://doi.org/10.1093/mnras/staa2450)
- Lu, W., & Piro, A. L. 2019, *ApJ*, 883, 40, doi: [10.3847/1538-4357/ab3796](https://doi.org/10.3847/1538-4357/ab3796)
- Lyu, F., Meng, Y.-Z., Tang, Z.-F., et al. 2021, *Frontiers of Physics*, 16, 24503, doi: [10.1007/s11467-020-1039-4](https://doi.org/10.1007/s11467-020-1039-4)
- Lyutikov, M., Barkov, M. V., & Giannios, D. 2020, *ApJL*, 893, L39, doi: [10.3847/2041-8213/ab87a4](https://doi.org/10.3847/2041-8213/ab87a4)
- Marcote, B., Paragi, Z., Hessels, J. W. T., et al. 2017, *ApJL*, 834, L8, doi: [10.3847/2041-8213/834/2/L8](https://doi.org/10.3847/2041-8213/834/2/L8)
- Metzger, B. D., Margalit, B., & Sironi, L. 2019, *MNRAS*, 485, 4091, doi: [10.1093/mnras/stz700](https://doi.org/10.1093/mnras/stz700)
- Michilli, D., Seymour, A., Hessels, J. W. T., et al. 2018, *Nature*, 553, 182, doi: [10.1038/nature25149](https://doi.org/10.1038/nature25149)

- Murase, K., Kashiyama, K., & Mészáros, P. 2016, *MNRAS*, 461, 1498, doi: [10.1093/mnras/stw1328](https://doi.org/10.1093/mnras/stw1328)
- Oostrum, L. C., Maan, Y., van Leeuwen, J., et al. 2020, *A&A*, 635, A61, doi: [10.1051/0004-6361/201937422](https://doi.org/10.1051/0004-6361/201937422)
- Oppermann, N., Yu, H.-R., & Pen, U.-L. 2018, *MNRAS*, 475, 5109, doi: [10.1093/mnras/sty004](https://doi.org/10.1093/mnras/sty004)
- Palaniswamy, D., Li, Y., & Zhang, B. 2018, *ApJL*, 854, L12, doi: [10.3847/2041-8213/aaa63](https://doi.org/10.3847/2041-8213/aaa63)
- Petroff, E., Hessels, J. W. T., & Lorimer, D. R. 2019, *A&A Rv*, 27, 4, doi: [10.1007/s00159-019-0116-6](https://doi.org/10.1007/s00159-019-0116-6)
- Planck Collaboration, & et al. 2016, *A&A*, 594, A13, doi: [10.1051/0004-6361/201525830](https://doi.org/10.1051/0004-6361/201525830)
- Popov, M. V., & Stappers, B. 2007, *A&A*, 470, 1003, doi: [10.1051/0004-6361:20066589](https://doi.org/10.1051/0004-6361:20066589)
- Popov, S. B., & Postnov, K. A. 2013, arXiv e-prints, arXiv:1307.4924, <https://arxiv.org/abs/1307.4924>
- Priesskorn, Z., & Kaaret, P. 2012, *ApJ*, 755, 1, doi: [10.1088/0004-637X/755/1/1](https://doi.org/10.1088/0004-637X/755/1/1)
- Rajwade, K. M., Mickaliger, M. B., Stappers, B. W., et al. 2020, *MNRAS*, 495, 3551, doi: [10.1093/mnras/staa1237](https://doi.org/10.1093/mnras/staa1237)
- Ravi, V. 2019, *Nature Astronomy*, 405, doi: [10.1038/s41550-019-0831-y](https://doi.org/10.1038/s41550-019-0831-y)
- Scholz, P., Spitler, L. G., Hessels, J. W. T., et al. 2016, *ApJ*, 833, 177, doi: [10.3847/1538-4357/833/2/177](https://doi.org/10.3847/1538-4357/833/2/177)
- Scholz, P., Bogdanov, S., Hessels, J. W. T., et al. 2017, *ApJ*, 846, 80, doi: [10.3847/1538-4357/aa8456](https://doi.org/10.3847/1538-4357/aa8456)
- Spitler, L. G., Cordes, J. M., Hessels, J. W. T., et al. 2014, *ApJ*, 790, 101, doi: [10.1088/0004-637X/790/2/101](https://doi.org/10.1088/0004-637X/790/2/101)
- Spitler, L. G., Scholz, P., Hessels, J. W. T., et al. 2016, *Nature*, 531, 202, doi: [10.1038/nature17168](https://doi.org/10.1038/nature17168)
- Spitler, L. G., Herrmann, W., Bower, G. C., et al. 2018, *ApJ*, 863, 150, doi: [10.3847/1538-4357/aad332](https://doi.org/10.3847/1538-4357/aad332)
- Tabor, E., & Loeb, A. 2020, *ApJL*, 902, L17, doi: [10.3847/2041-8213/abba79](https://doi.org/10.3847/2041-8213/abba79)
- Tendulkar, S. P., Bassa, C. G., Cordes, J. M., et al. 2017a, *ApJL*, 834, L7, doi: [10.3847/2041-8213/834/2/L7](https://doi.org/10.3847/2041-8213/834/2/L7)
- . 2017b, *ApJL*, 834, L7, doi: [10.3847/2041-8213/834/2/L7](https://doi.org/10.3847/2041-8213/834/2/L7)
- Wada, T., Ioka, K., & Zhang, B. 2021, arXiv e-prints, arXiv:2105.14480, <https://arxiv.org/abs/2105.14480>
- Wadiasingh, Z., & Timokhin, A. 2019, *ApJ*, 879, 4, doi: [10.3847/1538-4357/ab2240](https://doi.org/10.3847/1538-4357/ab2240)
- Wang, F. Y., & Dai, Z. G. 2013, *Nature Physics*, 9, 465, doi: [10.1038/nphys2670](https://doi.org/10.1038/nphys2670)
- Wang, F. Y., Dai, Z. G., Yi, S. X., & Xi, S. Q. 2015, *ApJS*, 216, 8, doi: [10.1088/0067-0049/216/1/8](https://doi.org/10.1088/0067-0049/216/1/8)
- Wang, F. Y., Wang, Y. Y., Yang, Y.-P., et al. 2020, *ApJ*, 891, 72, doi: [10.3847/1538-4357/ab74d0](https://doi.org/10.3847/1538-4357/ab74d0)
- Wang, F. Y., & Yu, H. 2017, *JCAP*, 03, 023, doi: [10.1088/1475-7516/2017/03/023](https://doi.org/10.1088/1475-7516/2017/03/023)
- Wang, F. Y., & Zhang, G. Q. 2019, *ApJ*, 882, 108, doi: [10.3847/1538-4357/ab35dc](https://doi.org/10.3847/1538-4357/ab35dc)
- Xiao, D., Wang, F., & Dai, Z. 2021, arXiv e-prints, arXiv:2101.04907, <https://arxiv.org/abs/2101.04907>
- Yang, H., & Zou, Y.-C. 2020, *ApJL*, 893, L31, doi: [10.3847/2041-8213/ab800f](https://doi.org/10.3847/2041-8213/ab800f)
- Yang, S., Yan, D., Dai, B., et al. 2019, *MNRAS*, 489, 2685, doi: [10.1093/mnras/stz2302](https://doi.org/10.1093/mnras/stz2302)
- Yang, Y.-H., Zhang, B.-B., Lin, L., et al. 2021, *ApJL*, 906, L12, doi: [10.3847/2041-8213/abd02a](https://doi.org/10.3847/2041-8213/abd02a)
- Yang, Y.-P., & Zhang, B. 2018, *ApJ*, 868, 31, doi: [10.3847/1538-4357/aae685](https://doi.org/10.3847/1538-4357/aae685)
- . 2021, arXiv e-prints, arXiv:2104.01925, <https://arxiv.org/abs/2104.01925>
- Yi, S.-X., Xi, S.-Q., Yu, H., et al. 2016, *ApJS*, 224, 20, doi: [10.3847/0067-0049/224/2/20](https://doi.org/10.3847/0067-0049/224/2/20)
- Zanazzi, J. J., & Lai, D. 2020, *ApJL*, 892, L15, doi: [10.3847/2041-8213/ab7cdd](https://doi.org/10.3847/2041-8213/ab7cdd)
- Zhang, B. 2018, *ApJL*, 867, L21, doi: [10.3847/2041-8213/aae8e3](https://doi.org/10.3847/2041-8213/aae8e3)
- . 2020, *Nature*, 587, 45, doi: [10.1038/s41586-020-2828-1](https://doi.org/10.1038/s41586-020-2828-1)
- Zhang, G. Q., Wang, F. Y., & Dai, Z. G. 2019, arXiv e-prints, arXiv:1903.11895, <https://arxiv.org/abs/1903.11895>
- Zhang, R. C., Zhang, B., Li, Y., & Lorimer, D. R. 2021, *MNRAS*, 501, 157, doi: [10.1093/mnras/staa3537](https://doi.org/10.1093/mnras/staa3537)
- Zhang, Y. G., Gajjar, V., Foster, G., et al. 2018, *ApJ*, 866, 149, doi: [10.3847/1538-4357/aadf31](https://doi.org/10.3847/1538-4357/aadf31)

Data set	r (day $^{-1}$)	k
All bursts	$734.47^{+29.04}_{-27.58}$	$0.72^{+0.01}_{-0.02}$
low-energy bursts	$445.35^{+30.42}_{-31.59}$	$0.69^{+0.02}_{-0.02}$
high-energy bursts	$354.74^{+27.14}_{-26.14}$	$0.76^{+0.03}_{-0.03}$
late-phase bursts	$800.54^{+48.84}_{-48.32}$	$0.66^{+0.02}_{-0.02}$
Oppermann et al. (2018)	$5.7^{+3.0}_{-2.0}$	$0.34^{+0.06}_{-0.05}$
Gourdji et al. (2019)	294^{+57}_{-52}	$0.82^{+0.12}_{-0.09}$
Oostrum et al. (2020)	$6.9^{+1.9}_{-1.5}$	$0.49^{+0.05}_{-0.05}$
Cruces et al. (2021)	74^{+31}_{-22}	$0.62^{+0.10}_{-0.09}$

Table 1. The best-fitting results of Weibull distribution for different samples. Waiting times with $\delta_t > 0.5$ day and $\delta_t < 30$ ms are excluded. The classification of low-energy bursts, high-energy bursts, and late-phase bursts is given in Section 3.2.

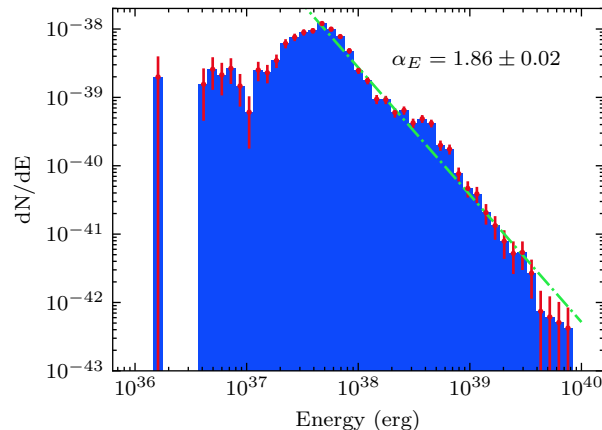


Figure 1. The differential energy distribution of FRB 121102. The blue histogram is the energy distribution and the red points and red vertical lines are the values and 1σ uncertainties. We use equation (1) to fit the energy distribution in the high-energy range ($E > 10^{38}$ erg) and show the best-fitting result as dot-dashed green line. The power-law index is -1.86 ± 0.02 . The bursts in the low energies deviate from power-law form.

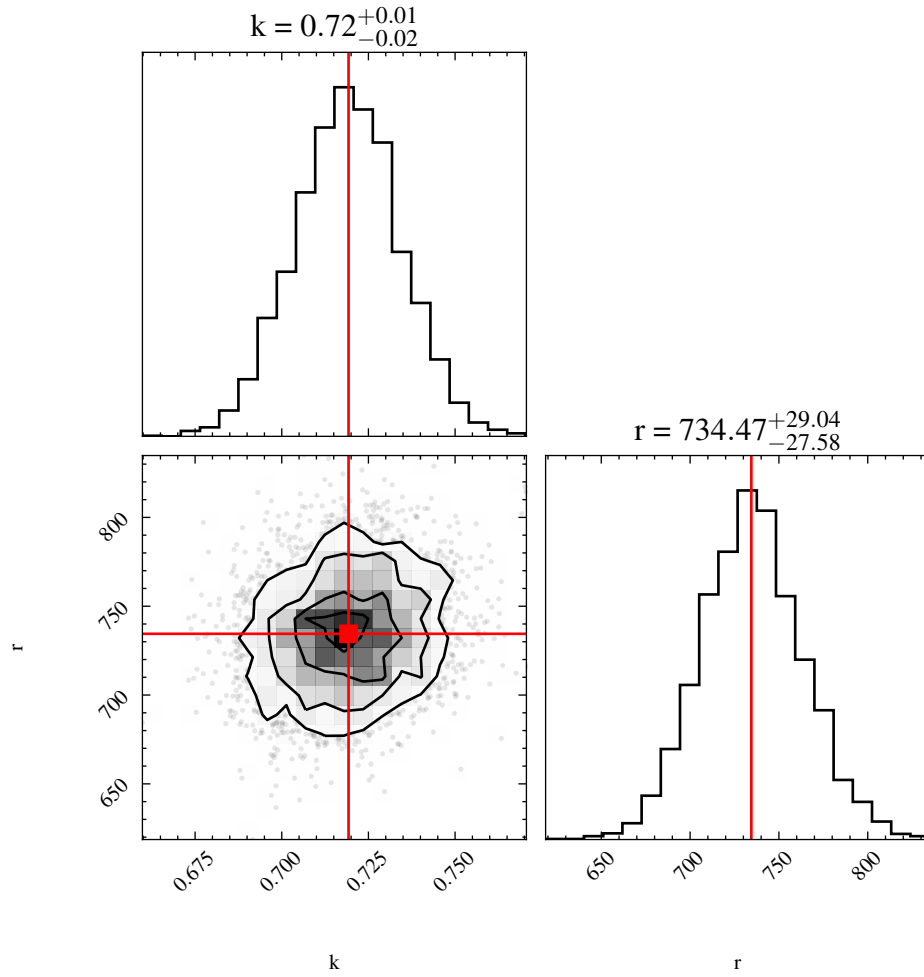


Figure 2. The corner plot for the shape parameter k and the event rate r for the Weibull distribution. The waiting times with $\delta_t < 30$ ms and $\delta_t > 0.5$ day are excluded. The best-fitting results are $k = 0.72^{+0.01}_{-0.01}$ and $r = 734.47^{+29.04}_{-27.58}$ per day.

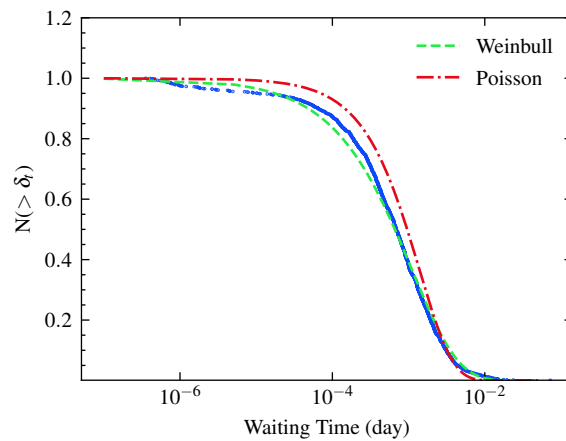


Figure 3. The cumulative distribution of waiting time. The blue scatter is the burst waiting time distribution. The dashed green lines and dot-dashed red lines are best-fit Weibull distribution and Poisson distribution, respectively. The Weibull distribution fit is better.

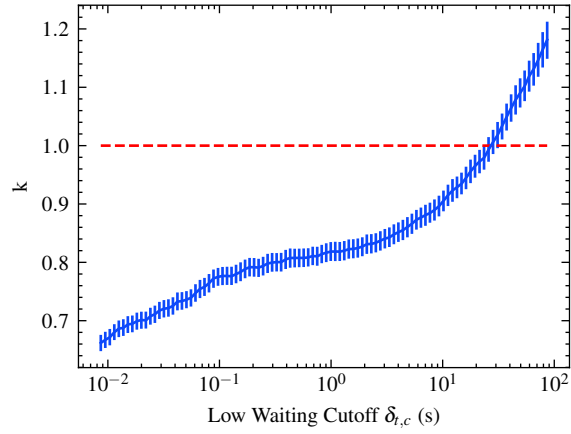


Figure 4. The shape parameter k against the low-waiting-time cutoff $\delta_{t,c}$ for Weibull distribution. The best-fitting results of the Weibull function with $\delta_t > \delta_{t,c}$ are derived. We select some different $\delta_{t,c}$ and show the shape parameters k in blue lines. The blue vertical lines are 1σ uncertainties. The dashed red line is $k = 1$. We found that the burst behavior closes to a Poisson process when $\delta_{t,c} = 28$ s. The best-fitting k increases as $\delta_{t,c}$ increases.

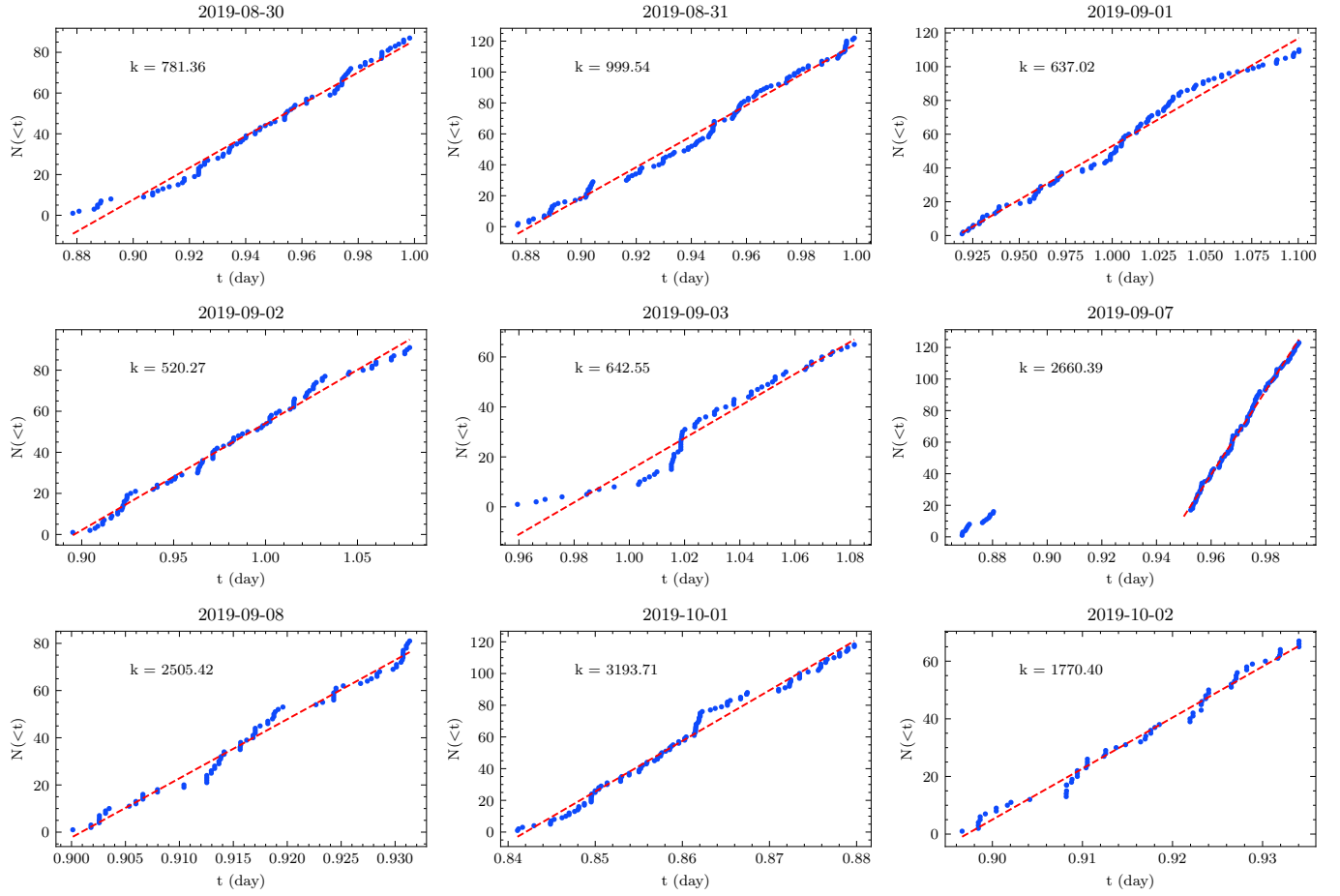


Figure 5. The cumulative distribution of burst number in single days. We select the days with the number of bursts greater than 60. In all cases, the distribution can be well fitted with $N(<t) = kt + b$. The best-fitting results are shown as dashed red lines in each panel.

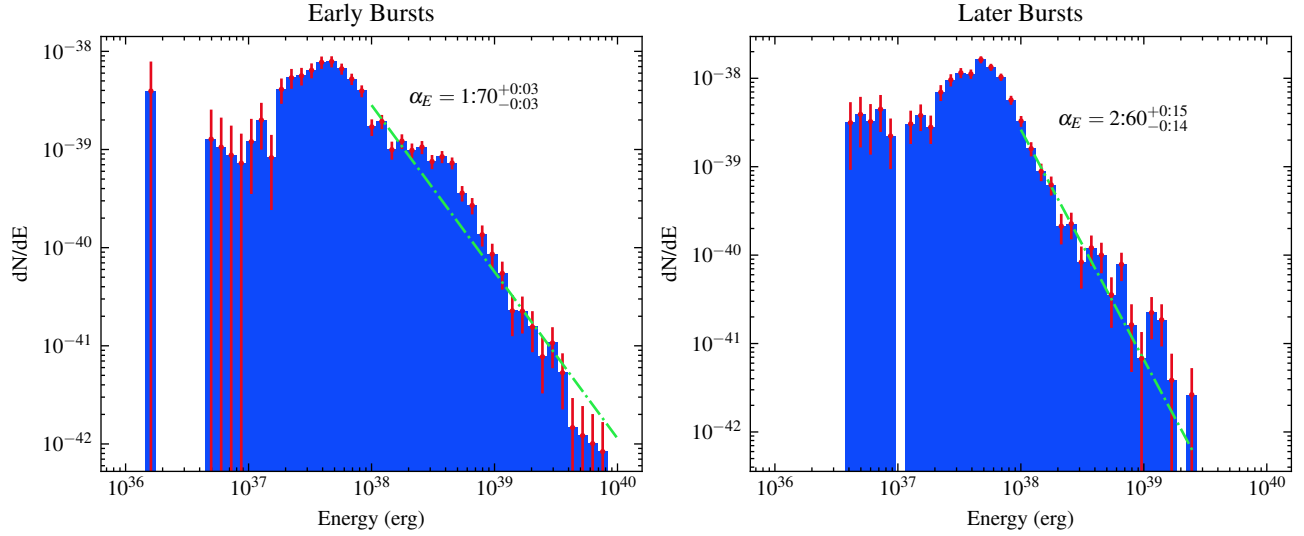


Figure 6. The energy distribution of bursts in different epochs. The early bursts refer to that the bursts occurred before MJD 58740 and the late bursts refer to those occurring after MJD 58740. We use the simple power law to fit the bursts with energy greater than 10^{38} erg. The dot-dashed green lines are the best-fitting results. The power-law indices are also shown in each panel.

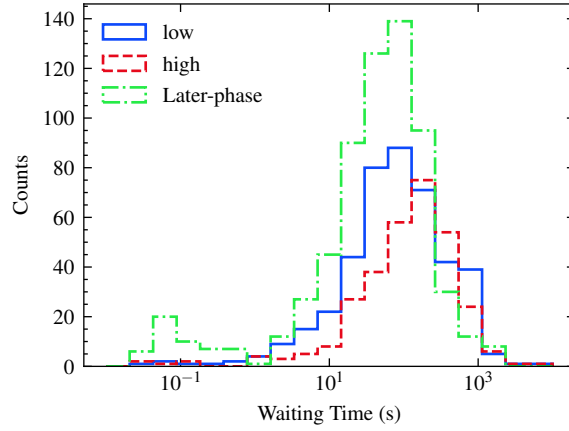


Figure 7. The histograms of waiting times for three sub-samples. According to the bimodal structure in [Li et al. \(2021\)](#), we divide the bursts into 3 sub-samples: the low-energy bursts and high-energy bursts from 58717 to 58740, and the late-phase bursts. The peak of the low-energy bursts and the late-phase bursts are consistent with each other, while the peak of the high-energy bursts is slightly higher.

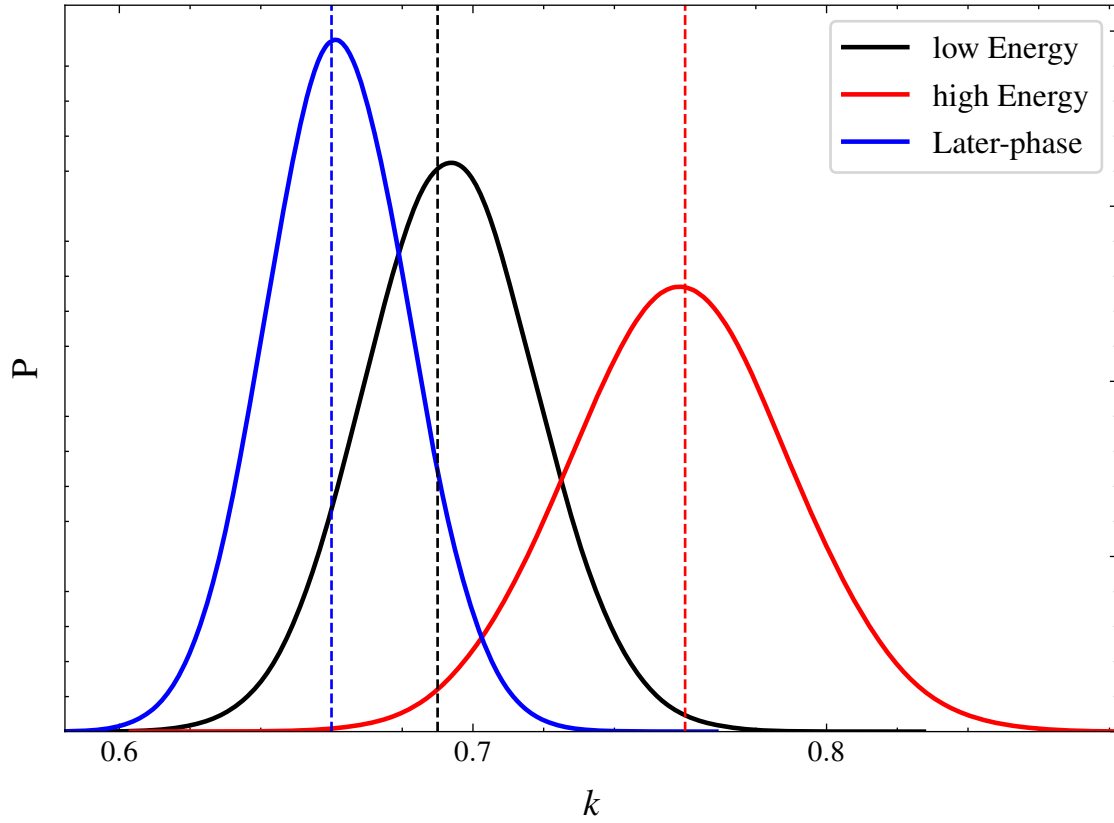


Figure 8. The shape parameter k for the three sub-samples. The solid lines are the posterior probability distributions of the k parameter for the three sub-samples, and the dashed lines indicate the mean values of the posterior distribution. The value of k for low-energy bursts and late-phase bursts are consistent. However, the value of k for high-energy bursts is slightly higher.

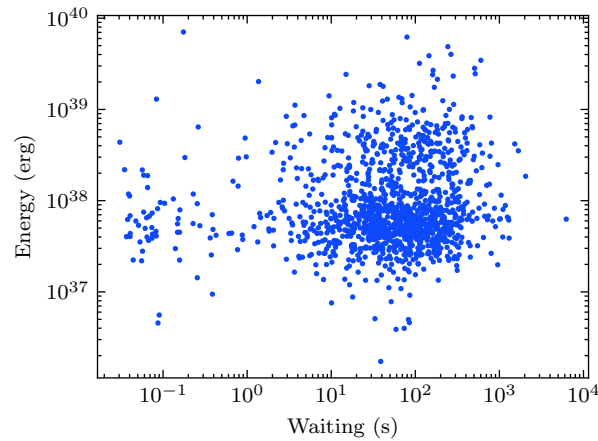


Figure 9. Scatter plot between waiting time and the energy of the burst after the waiting time. There is no correlation between burst energy and waiting time.

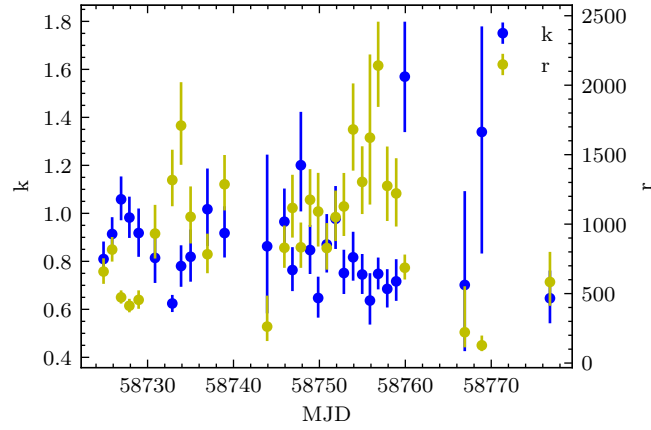


Figure 10. Shape parameters k and burst rate r in single days with the burst number greater than 5. The blue points are the shape parameters k with 1σ errors, while the yellow points are the burst rate r with 1σ errors. The event rate r changes significantly across observing time, while the shape parameter k varies slightly in different days. It is interesting to see that the value of k is close to 1 in some days.